

Slow Modes of the Equatorial Waveguide

KERRY EMANUEL

Lorenz Center, Massachusetts Institute of Technology, Cambridge, Massachusetts

(Manuscript received 10 October 2019, in final form 16 February 2020)

ABSTRACT

A recently developed linear model of eastward-propagating disturbances has two separate unstable modes: convectively coupled Kelvin waves destabilized by the wind dependence of the surface enthalpy flux, and slow, MJO-like modes destabilized by cloud–radiation interaction and driven eastward by surface enthalpy fluxes. This latter mode survives the weak temperature gradient (WTG) approximation and has a time scale dictated by the time it takes for surface fluxes to moisten tropospheric columns. Here we extend that model to include higher-order modes and show that planetary-scale low-frequency waves with more complex structures can also be amplified by cloud–radiation interactions. While most of these waves survive the WTG approximation, their frequencies and growth rates are seriously compromised by that approximation. Applying instead the assumption of zonal geostrophy results in a better approximation to the full spectrum of modes. For small cloud–radiation and surface flux feedbacks, Kelvin waves and equatorial Rossby waves are destabilized, but when these feedbacks are strong enough, the frequencies do not lie close to classical equatorial dispersion curves except in the case of higher-frequency Kelvin and Yanai waves. An eastward-propagating $n = 1$ mode, in particular, has a structure resembling the observed structure of the MJO.


1. Introduction

Intraseasonal variations of clouds, precipitation, and winds in the equatorial atmosphere are concentrated at low frequencies and zonal wavenumbers, as revealed by wavenumber–frequency spectra of outgoing long-wave radiation (OLR; [Wheeler and Kiladis 1999](#)). Perturbations away from this smooth, red spectrum seem to fall along the linear dispersion curves of equatorially trapped waves, first derived more than a half century ago by [Matsuno \(1966\)](#). Yet the most prominent such perturbation, the Madden–Julian oscillation (MJO), does not fall along any such dispersion curve and is more closely characterized by constant frequency. Numerical simulations ([Arnold and Randall 2015](#); [Khairoutdinov and Emanuel 2018](#), hereafter [KE18](#); [Kim et al. 2011](#)) suggest that the MJO is an example of self-aggregation of convection, amplified by the interaction of radiation with clouds and water vapor and driven eastward by variable surface enthalpy fluxes and/or horizontal advection of water vapor.

[Arnold and Randall \(2015\)](#) analyzed simulations on an aquaplanet with uniform sea surface temperature using the superparameterized Community Atmosphere Model (SP-CAM), which employs a superparameterization of moist convection. Their MJO-like disturbance nearly disappears when radiative cooling is horizontally homogenized, and they concluded that these disturbances are driven eastward by the wind-induced surface heat exchange (WISHE) mechanism. This is consistent with earlier results from mechanism denial experiments conducted by [Kim et al. \(2011\)](#), who used an atmospheric general circulation model with parameterized convection and prescribed sea surface temperature.

[KE18](#) performed simulations using a cloud-permitting model in an equatorially centered channel extending to $\pm 46^\circ$ latitude, with fixed, spatially constant surface temperature and no land. These displayed a rich spectrum of equatorial variability, including an MJO-like mode that disappeared when radiation was horizontally homogenized and whose eastward propagation ceased when surface fluxes were homogenized. The spectra also exhibited OLR minima aligned along the classical Matsuno dispersion curves, including some signals near the equatorial Rossby wave dispersion curves.

To help interpret their results, [KE18](#) proposed a linear model of disturbances on an equatorial beta plane that

 Denotes content that is immediately available upon publication as open access.

Corresponding author: Kerry Emanuel, emanuel@mit.edu

follows in the footsteps of earlier, similar work by [Fuchs and Raymond \(2005\)](#), [Bony and Emanuel \(2005\)](#), [Zurovac-Jevtić et al. \(2006\)](#), and [Fuchs and Raymond \(2017\)](#). These models all suggest that the MJO is driven by some combination of cloud–radiation interaction and WISHE. [Fuchs and Raymond \(2005\)](#) concluded that the main driver of the MJO is cloud–radiation interaction, while WISHE is responsible for its eastward propagation. But in their updated analysis, [Fuchs and Raymond \(2017\)](#) identified WISHE as the main mechanism for driving the MJO, though cloud–radiation interactions further destabilized the model. This is also consistent with mechanism denial experiments conducted with an atmospheric general circulation model with fixed, constant sea surface temperature, by [Shi et al. \(2018\)](#). [KE18](#)'s linear model showed an MJO-like mode destabilized by cloud–radiation interaction and driven eastward by WISHE, and Kelvin modes driven mostly by WISHE. Only the MJO-like mode survives a weak temperature gradient (WTG) approximation to the full linear equations.

The linear model developed by [KE18](#) was solved only for the special case of no meridional wind. Our purpose here is to extend that analysis to higher-order modes and to explore the extent to which they can be approximated using the WTG formalism and/or the assumption of geostrophy of the zonal wind.

2. Linear model

The linear model of [KE18](#) is based on the assumption that on the scales of interest, the vertical virtual temperature profile of the tropical atmosphere is always moist adiabatic, that the motions are hydrostatic and that the vertical velocity vanishes at the tropopause. If these assumptions are satisfied, and the flow is hydrostatic, the vertical structure of tropospheric disturbances is constrained to the first baroclinic mode ([Emanuel 1987](#); [Neelin and Yu 1994](#)), having the mathematical form of the shallow water equations. The assumption of a rigid lid is, however, poor, particularly for higher-frequency disturbances ([Chumakova et al. 2013](#); [Yano and Emanuel 1991](#)). Replacing the rigid lid by a passive stratosphere with a wave radiation boundary condition imposed at its top is straightforward but algebraically complex, and [KE18](#) elected to use a rigid lid but emulate wave radiation by imposing a frequency-dependent damping. We here use the same approximation and note that it is likely to be reasonably well satisfied for the low-frequency disturbances considered here. It should be noted, however, that observations, particularly of the faster modes such as equatorial Kelvin waves, do not resemble first baroclinic mode structures, perhaps

because such modes in reality leak energy into the stratosphere fairly rapidly, changing the structure of the disturbances in the troposphere, or because of departures from strict moist adiabatic profiles.

The nondimensional form of the [KE18](#)'s linear equations are repeated here:

$$\frac{\partial u}{\partial t} = \frac{\partial s}{\partial x} + yv, \quad (1)$$

$$\frac{\partial v}{\partial t} = \delta \left(\frac{\partial s}{\partial y} - yu \right), \quad (2)$$

$$\frac{\partial u}{\partial x} + \frac{\partial v}{\partial y} + w = 0, \quad (3)$$

$$\frac{\partial s}{\partial t} = Cs_m - w + s_m - \chi s - \alpha u, \quad (4)$$

$$\gamma \frac{\partial s_m}{\partial t} = -Ds - \alpha u + \kappa Cs_m - Gw + d \frac{\partial^2 s_m}{\partial x^2}. \quad (5)$$

Here u , v , and w are the zonal, meridional, and vertical perturbations velocities, s is the saturation entropy of the troposphere, and s_m is the moist entropy vertically averaged through the troposphere. It has been assumed that the background surface wind is easterly in deriving the last term in (4) and the second term on the right-hand side of (5). Although the observed zonal mean zonal wind in the tropics is easterly at all times of the year, there are bands of longitude in which the mean flow is westerly, particularly in the eastern equatorial Indian and western Pacific Oceans, and particularly in boreal winter. This may be one of the most consequential differences from aquaplanet simulations, in which the equatorial zonal flow is easterly at all longitudes.

These equations are very similar to, but not identical to (7)–(12) of [Fuchs and Raymond \(2005\)](#).

The nondimensional coefficients in (1)–(5) are as follows: δ determines the degree of zonal geostrophy, C is the magnitude of the cloud–radiative feedback, χ and D measure the damping effect of boundary layer entropy perturbations on surface fluxes, α governs the magnitude of the WISHE feedback, G is a normalized gross moist stability, and d is the normalized Fickian diffusion coefficient. The factors γ and κ account for the different ways that s and s_m have been scaled. The precise definitions of these coefficients are given in the appendix of [KE18](#) together with the scales used to nondimensionalize the equations. For Earthlike conditions, the characteristic zonal scale is the radius of Earth, about 6400 km, the characteristic meridional scale is around 750 km and a characteristic time scale is around 4 days.

Before proceeding with a detailed analysis, we derive a quasi-energy constraint by multiplying (1), (2), (4), and

(5) by their respective variables, summing them, and averaging the result over the whole spatial domain, assuming that the variables vanish at $y = \pm\infty$. We define an averaging operator $\{\dots\}$:

$$\{p\} \equiv \int_{-\infty}^{\infty} \int_0^{2\pi} p \, dx \, dy.$$

The result is

$$\begin{aligned} \frac{\partial}{\partial t} \frac{1}{2} \left\{ u^2 + \frac{1}{\delta} v^2 + s^2 + \gamma \frac{1+C}{D} s_m^2 \right\} = & -\alpha \left\{ us + \frac{1+C}{D} us_m \right\} + \frac{1+C}{D} \kappa C \{s_m^2\} - G \frac{1+C}{D} \{ws_m\} - \chi \{s^2\} \\ & - d \frac{1+C}{D} \left\{ \left(\frac{\partial s_m}{\partial x} \right)^2 \right\}. \end{aligned} \tag{6}$$

In deriving (6), the factor $(1 + C)/D$ was introduced to eliminate a term involving a correlation between s and s_m and use has been made of (3).

For growing modes, the right-hand side of (6) must be positive. The first term on the right of (6) is the WISHE effect and can only produce growth (for background easterlies, for which $\alpha > 0$) when the zonal velocity perturbation is negatively correlated with s , s_m , or both. The second term on the right is the positive feedback from clouds interacting with longwave radiation, which requires both κ and C to be positive. The sign of the third term is not a priori obvious, although moisture anomalies, as represented by s_m are generally positively correlated with vertical velocity, so that term will usually be negative, but it is not always negative in what follows. The last two terms are damping terms and are negative definite.

Thus, growth of disturbances in this model requires WISHE and/or cloud–radiation feedback, unless a mode can arise in which vertical velocity is negatively correlated with midtropospheric moisture.

Next, we eliminate all the variables in (1)–(5) in favor of the meridional velocity v and we look for normal-mode solutions of the form

$$v = \text{Real}[V(y)e^{ikx+\sigma t}], \tag{7}$$

where $V(y)$ is a complex function, k is the zonal wavenumber ($k = 1, 2, 3, \dots$) and σ is a complex growth rate. This yields an ordinary differential equation for $V(y)$:

$$\begin{aligned} \sigma a_3 \frac{d^2 V}{dy^2} - a_2 y \frac{dV}{dy} + \left[ika_3 - a_2 - \frac{\sigma}{\delta} (a_1 \sigma + ika_2 + k^2 a_3) \right. \\ \left. - a_1 y^2 \right] V = 0, \end{aligned} \tag{8}$$

where

$$\begin{aligned} a_1 &\equiv D(1 + C) + (\chi + \sigma)(\gamma\sigma + dk^2 - \kappa C), \\ a_2 &\equiv \alpha(\gamma\sigma + dk^2 - \kappa C + 1 + C), \\ a_3 &\equiv \gamma\sigma + dk^2 - \kappa C + G(1 + C). \end{aligned} \tag{9}$$

As can be verified by substitution, (8) has solutions have the form

$$V_n = H_n(y)e^{-by^2}, \tag{10}$$

where the complex exponential coefficient b is given by

$$b = \frac{-a_2 \pm \sqrt{a_2^2 + 4\sigma a_1 a_3}}{4\sigma a_3}, \tag{11}$$

and H_n are Hermite polynomials whose first four terms are

$$\begin{aligned} H_0 &= 1, \\ H_1 &= y, \\ H_2 &= \frac{1}{2}y^2 + c_1, \\ H_3 &= \frac{1}{3}y^3 + c_2 y. \end{aligned} \tag{12}$$

Note that the solutions (10) form a complete set; any arbitrary initial perturbation can be described as a sum over these modes. The constants that appear in (12) are

$$\begin{aligned} c_1 &= \frac{\sigma a_3}{(2b\sigma - ik)a_3 + a_2 + \frac{\sigma}{\delta} (a_1 \sigma + ika_2 + k^2 a_3)}, \\ c_2 &= \frac{2\sigma a_3}{(6b\sigma - ik)a_3 + 2a_2 + \frac{\sigma}{\delta} (a_1 \sigma + ika_2 + k^2 a_3)}. \end{aligned} \tag{13}$$

The coefficients in (8) must also satisfy the dispersion relation

$$\begin{aligned} \frac{1}{2}a_2 - ika_3 + \frac{\sigma}{\delta} (a_1 \sigma + ika_2 + k^2 a_3) \\ \pm \left(n + \frac{1}{2} \right) \sqrt{a_2^2 + 4\sigma a_1 a_3} = 0, \end{aligned} \tag{14}$$

in which $n = 0, 1, 2, 3, \dots$, corresponding to the order of the Hermite polynomials in (12). The choice of sign in

the square root in (14) must match that of (11). To satisfy the boundary conditions at $y = \pm\infty$ the real part of b must be positive; any roots of (14) that do not satisfy this condition are discarded.

When (14) is expanded, it becomes apparent that it is an eighth-order polynomial equation for the complex growth rate σ . Fuchs and Raymond (2005) also derived an eighth-order dispersion relation. Owing to the algebraic complexity of the equation, it is solved using the “solve” function of MATLAB and rigorously checked against direct solutions in certain limiting cases.¹ In practice, for each combination of parameters and each zonal wavenumber k we have examined, there are at most two roots that exhibit positive growth and that satisfy the boundary conditions at $y = \pm\infty$. If there are two roots, we show only the most rapidly growing in most of what follows.

The set (1)–(5) also admits solutions for which $v = 0$ and these were derived and discussed by KE18. The dispersion relation is cubic in this case. Note that these solutions obey exact zonal geostrophy, according to (2). Following convention, we also refer to this as the $n = -1$ mode.

The parameter δ that appears in (2) is typically large [$O(\sim 30)$], which suggests that modes of reasonably low [$O(\sim 1)$] nondimensional frequency may exhibit approximate zonal geostrophy. If we take the limit as $\delta \rightarrow \infty$ in (14), the dispersion relation becomes quartic and it is less taxing to write out an explicit polynomial equation for the complex growth rate. That dispersion relation is solved using a polynomial root solver, and as before, roots are discarded that fail to obey the boundary conditions at $y = \pm\infty$. These geostrophic solutions can then be compared to solutions of the complete set.

To derive a consistent WTG approximation to (1)–(5) we first develop a vorticity equation by cross differentiating (1)–(2):

$$\frac{\partial}{\partial t} \left(\frac{1}{\delta} \frac{\partial v}{\partial x} - \frac{\partial u}{\partial y} \right) = -y \left(\frac{\partial u}{\partial x} + \frac{\partial v}{\partial y} \right) - v. \quad (15)$$

We then set $s = 0$ in (4) and (5), so that the WTG equations consist of (6) together with

$$\frac{\partial u}{\partial x} + \frac{\partial v}{\partial y} + w = 0, \quad (16)$$

$$(1 + C)s_m = w + \alpha u, \quad (17)$$

and

$$\gamma \frac{\partial s_m}{\partial t} = -\alpha u + \kappa C s_m - Gw + d \frac{\partial^2 s_m}{\partial x^2}. \quad (18)$$

We look for solutions in the limit $\delta \rightarrow \infty$ satisfying the boundary condition that the perturbations vanish as $y \rightarrow \pm\infty$. Repeating the derivation as before, the dispersion relation is linear in this case and we write explicit relations for growth rates and phases speeds:

$$\gamma \sigma_r = \kappa C - dk^2 - (1 + C) \frac{n^2 \alpha^2 + Gk^2}{n^2 \alpha^2 + k^2} \quad (19)$$

and

$$\gamma c = -\frac{\gamma \sigma_i}{k} = \frac{-n\alpha(1 + C)(1 - G)}{n^2 \alpha^2 + k^2}. \quad (20)$$

When $n = -1$ these relationships are identical to those derived by KE18 and the disturbances propagate eastward. All the other modes (in terms of n) propagate westward. These solutions satisfy the boundary conditions in y but note that $k = 0$ does not satisfy the boundary conditions and is thus excluded. Nor are there viable solutions that satisfy the boundary conditions for $n = 0$.

One curious feature of the solution is that the dispersion relationships for $n = -1$ and $n = 1$ are identical except that the propagation directions are opposite.

From (20), propagation requires WISHE ($\alpha \neq 0$), while (19) shows that wave growth is impeded by WISHE. There are no solutions for $\alpha < 0$ (westerly mean surface wind) that satisfy the boundary conditions.

For all the WTG modes, growth is only possible when both κ and the cloud–radiation feedback parameter C are sufficiently large, depending on the values of n and k . The definition of κ from the appendix of KE18 is

$$\kappa \equiv \varepsilon_p H \frac{d\bar{s}_d}{dz} \frac{1}{\bar{s}^* - \bar{s}_m}, \quad (21)$$

where ε_p is the precipitation efficiency, H is a scale height of the troposphere, \bar{s}_d is the mean-state dry entropy, \bar{s}^* is the saturation entropy of the troposphere, and \bar{s}_m is the tropospheric mean value of the moist entropy. Along a moist adiabat, $H d\bar{s}_d/dz \cong L_v q^*/T$, where L_v is the latent heat of vaporization, q^* is a characteristic value of the saturation specific humidity, and T is a representative temperature. Likewise, $\bar{s}^* - \bar{s}_m \cong L_v q^*(1 - \mathcal{H})/T$, where \mathcal{H} is a characteristic value of relative humidity in the free troposphere. Thus, we have

$$\kappa \cong \frac{\varepsilon_p}{1 - \mathcal{H}}. \quad (22)$$

¹The reader interested in exploring the parameter space of this model may download a MATLAB script to do so (from <ftp://texmex.mit.edu/pub/emanuel/scripts/equapak.zip>).

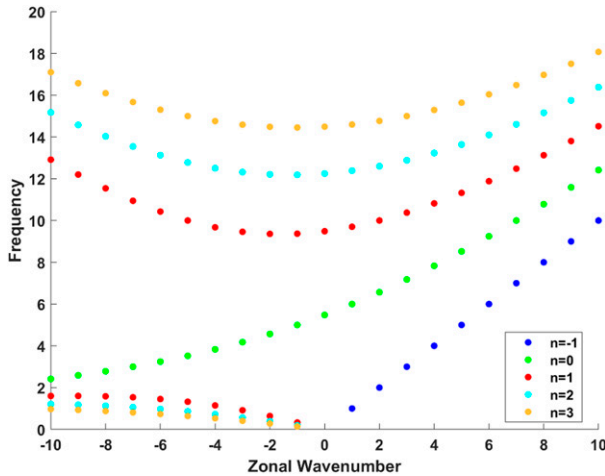


FIG. 1. Solutions for the frequency as a function of zonal-wavenumber and meridional mode number in the classical limit of vanishing forcing and dissipation, and taking $G = 0$ and $\delta = 30$. The colors indicate the meridional mode as indicated in the legend.

3. Solutions

We first present solutions of the full dispersion relationship in (14), subject to the condition that the real part of b given by (11) is positive so that the solutions are well behaved at $y = \pm\infty$. As a partial test of the solver, we first examine the case of vanishing forcing and dissipation: $\alpha = C = \chi = D = d = 0$, and we also take $G = 0$ to reduce (1)–(5) to the classical Matsuno problem. Here, in our case, the solution is a function of the single nondimensional parameter δ , which we take to be 30. In this case, the real part of the growth rates vanishes and all the modes are neutral. Figure 1 shows the frequency

as a function of zonal wavenumber for the first four meridional modes plus the special solution for the $v = 0$ mode, which by convention we label the $n = -1$ solution. Clearly the classical solutions are recovered in this case.

We next jump to values of the parameters that more nearly reflect actual conditions in the tropics. Specifically, we take $\alpha = 1.5$, $\gamma = 1$, $\kappa = 2$, $G = 0.1$, $C = 0.8$, $D = 1.5$, $\chi = 1.5$, $d = 0.02$, and $\delta = 30$. Figure 2a shows the dispersion relationship in this case, with only growing modes displayed and with the diameter of the dots proportional to the growth rates. Figure 2b simply zooms in on the lower-frequency modes. The size of the largest dot corresponds to a (nondimensional) growth rate of 0.96, for the $n = 1$ mode and for a westward-propagating zonal wavenumber of 2. The higher-frequency modes, with relatively modest growth rates, correspond fairly well with the Kelvin, mixed Rossby–gravity waves, and some eastward-propagating inertia–gravity waves seen in the Matsuno neutral solutions. These higher-frequency modes vanish when WISHE is absent ($\alpha = 0$) and may therefore be presumed to be destabilized by the WISHE mechanism, as in Emanuel (1993). But the more rapidly growing low-frequency modes occupy a narrow range of frequencies and do not correspond in any simple way to the classical neutral modes. For example, the group velocity of the low-frequency $v = 0$ ($n = -1$) mode (blue dots) is westward, and there are low-frequency eastward-propagating modes for $n > 0$. All of these low-frequency modes are destabilized by the cloud radiation term, as represented by the parameter C ; when this is set to zero (not shown) only the high-frequency WISHE modes remain. Thus the low-frequency modes in Fig. 2 are cloud–radiation modes in which the feedback is strong enough to drive the frequencies well away from

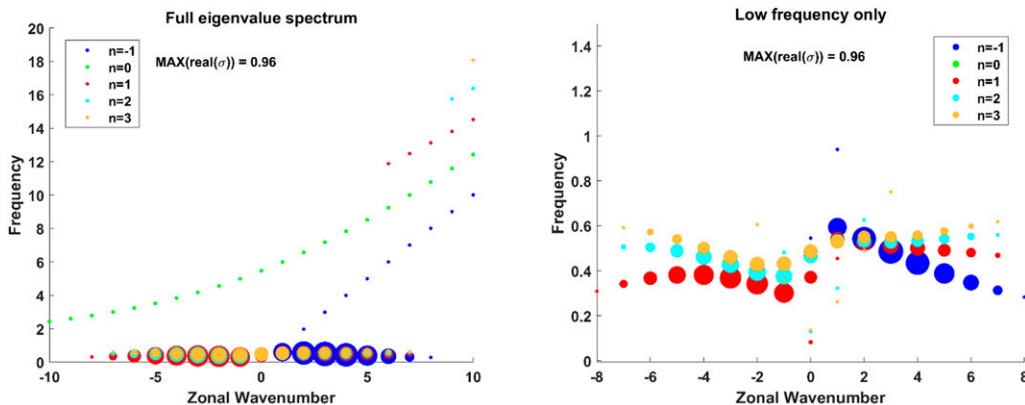


FIG. 2. (left) Solutions of the dispersion relation for $\alpha = 1.5$, $\gamma = 1$, $\kappa = 2$, $G = 0.1$, $C = 0.8$, $D = 1.5$, $\chi = 1.5$, $d = 0.02$, and $\delta = 30$. In this case, the diameters of the circles are proportional to the growth rates, with the largest circle corresponding to a growth rate of 0.96. (right) As in the left panel, but zooming in on the lower frequencies.

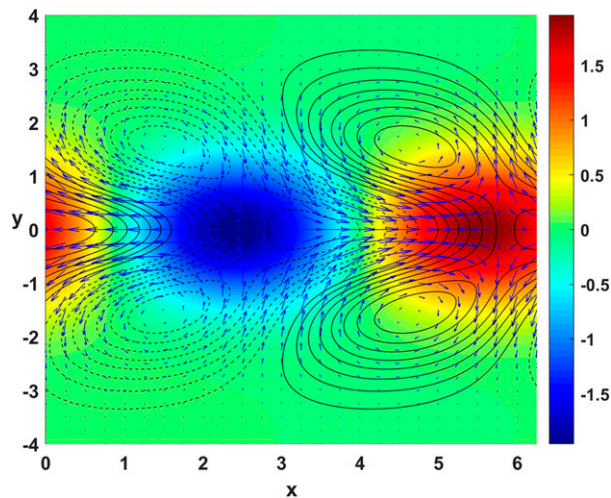


FIG. 3. Eigenfunction of the $n = 1$, $k = 3$ mode corresponding to the parameters used to construct Fig. 2. The colors show the vertical velocity, the arrows show the low-level perturbation horizontal winds, and the black contours show the distribution of saturation entropy s^* . Given typical Earthlike parameters, for an (arbitrary) peak zonal wind perturbation of 5 m s^{-1} , the peak meridional wind is about 0.5 m s^{-1} , the peak vertical wind is about 0.5 cm s^{-1} and the peak temperature perturbation is about 0.15 K .

the classical Matsuno solutions. Although they are amplified by radiative effects, their frequencies are strongly affected by WISHE.

This non-Matsuno character is evident also in the eigenfunctions. For example, Fig. 3 shows the spatial distribution of low-level perturbation wind, vertical velocity, and saturation entropy (our proxy for temperature) for the $n = 1$, $k = 3$ mode corresponding to the parameters used in Fig. 2. This mode has a nondimensional growth rate of about 0.7. Cyclonic gyres are found poleward and westward of the region of ascent, and the saturation entropy has maxima within the gyres and also along the equator just ahead of the region of maximum ascent. The convective mass flux (not shown here) strongly resembles the vertical velocity pattern. The $n = 1$ mode somewhat more closely resembles the structure of the observed MJO than does the $v = 0$ mode and has about the right (dimensional) eastward translation speed (roughly 7 m s^{-1} for typical values of the parameters, comparable to observed phase speeds of around 5 m s^{-1} , especially when the Doppler shift by the mean flow is accounted for). Compare the structure shown in Fig. 3 with the 200-hPa winds and MSU temperatures regressed onto low-frequency filtered OLR from Hendon and Liebmann (1994, their Fig. 2a reproduced here as Fig. 4), bearing in mind that winds at 200 hPa tend to be opposite to the winds in the lower troposphere that are shown in Fig. 3.

Figure 5, in the same format as Fig. 3, shows the structure of the most rapidly growing mode, with $n = 1$ and $k = -2$.

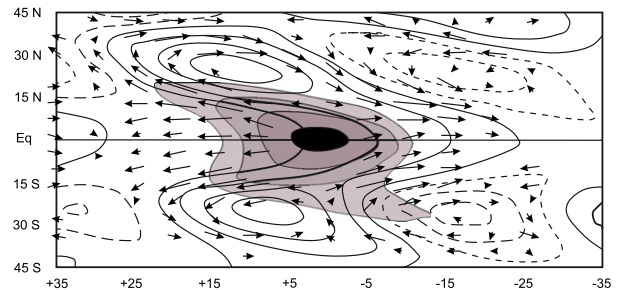


FIG. 4. Latitude-lag map of 200-hPa winds (vectors), Microwave Sounding Unit channel-2 temperature (MSUT; contours), and OLR (shaded) regressed onto OLR at 0°N , 125°E . All data are windowed according to significant activity at the equator and bandpass filtered to eastward wavenumbers 1–3 with 35–95-day periods. The regressed fields are shown for a one-standard-deviation fluctuation of the reference time series. Maximum vectors are 2.7 m s^{-1} . Contour interval for MSUT is $5.0 \times 10^{-2} \text{ K}$. Shading levels for OLR are 0.5, 1.75, 3.0, and 4.25 K . Figure after and caption from Hendon and Liebmann (1994).

This mode, traveling westward with a phase speed of around 5 m s^{-1} , also has trailing cyclonic vortices but they are more elongated and the whole mode is more confined close to the equator (compare the meridional scales of the two figures).

The effect on the dispersion curves of various approximations to the full linear equations is shown in Fig. 6. The left side of the figure compares the full dispersion solutions (Fig. 2) to the approximate solutions in the limit $\delta \rightarrow \infty$ while the right side makes the additional WTG approximation. In both cases, the approximate solutions are shown by open circles while filled circles show the full solution. The approximation of zonal geostrophy ($\delta \rightarrow \infty$) introduces relatively little distortion to the low-frequency dispersion solutions, but the WTG approximation does not work well for most of the modes displayed here. The eigenfunctions of the geostrophic solutions (not shown here) also closely resemble those of the full solutions.

The reader is invited to further explore the parameter space of these solutions and approximation to the solutions using software provided by the author (see footnote 1).

4. Discussion and summary

Numerical experiments using full-physics global and near-global models suggest that cloud–radiation interactions (Arnold and Randall 2015; KE18; Kim et al. 2011) and WISHE (Shi et al. 2018) are essential to low-frequency equatorial modes such as the MJO. When radiative heating and/or surface wind is horizontally homogenized in these models, the low-frequency modes largely or completely disappear. This suggests that we might

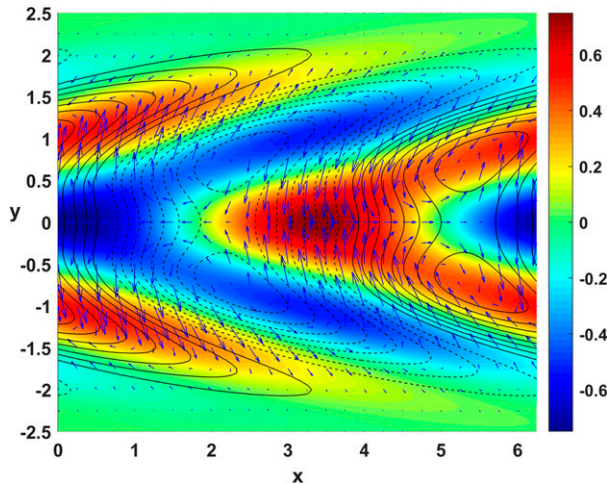


FIG. 5. As in Fig. 3, but showing the structure of a westward-propagating mode, with $n = 1$ and $k = -2$. Given typical Earthlike parameters, for an (arbitrary) peak zonal wind perturbation of 5 m s^{-1} , the peak meridional wind is about 1.5 m s^{-1} , the peak vertical wind is about 1 cm s^{-1} , and the peak temperature perturbation is about 0.25 K .

think of these low-frequency modes as manifestations of self-aggregation of moist convection on a sphere.

The present work extends the linear theory developed by KE18 to higher-order modes for which the meridional velocity does not vanish. The higher-frequency modes are destabilized by WISHE, but the low-frequency disturbances are driven by cloud–radiation interactions and are weakly damped by WISHE, though WISHE is essential to their propagation. For realistic values of the nondimensional parameters in the linear model, the cloud–radiation interaction drives the dispersion characteristics of the low-frequency modes well away from the neutral modes first derived by Matsuno (1966) so that it becomes

problematic if not meaningless to identify them with the neutral modes. In particular, some of the $n = 1$ eastward-propagating modes have structures that resemble that of the observed MJO (cf. Figs. 3 and 4).

An important limitation of this and indeed most linear models is the imposition of a rigid lid at the tropopause. As shown by Yano and Emanuel (1991), allowing upward wave propagation into the stratosphere damps modes more or less in proportion to their frequency. Here we emulated this effect with Fickian diffusion, which is far from satisfactory. Future work will attempt to match the tropospheric system developed here with a passive stratosphere and explore the effect of upward wave radiation on the growth rates, phase speeds and structure of solutions to the model. In particular, we expect that the solutions will exhibit vertical phase tilts that may prove to be more consistent with observations than are the rigid-lid solutions.

The cloud–radiation interaction has been represented here as proportional to the perturbation column moist entropy, a gross oversimplification of reality where the radiative effects of clouds are sensitive to the optical properties of the clouds as well as ensemble measures of cloud cover. If cloud–radiation interactions are indeed important for low-frequency variability of equatorially trapped disturbances, then the fidelity with which such variability can be simulated in global models must be sensitive to the model representation of clouds, including especially the thickness, lateral extent, and optical properties of high cirrus associated with deep convection. This may prove central to improving the simulation of low-frequency tropical modes in weather and climate models.

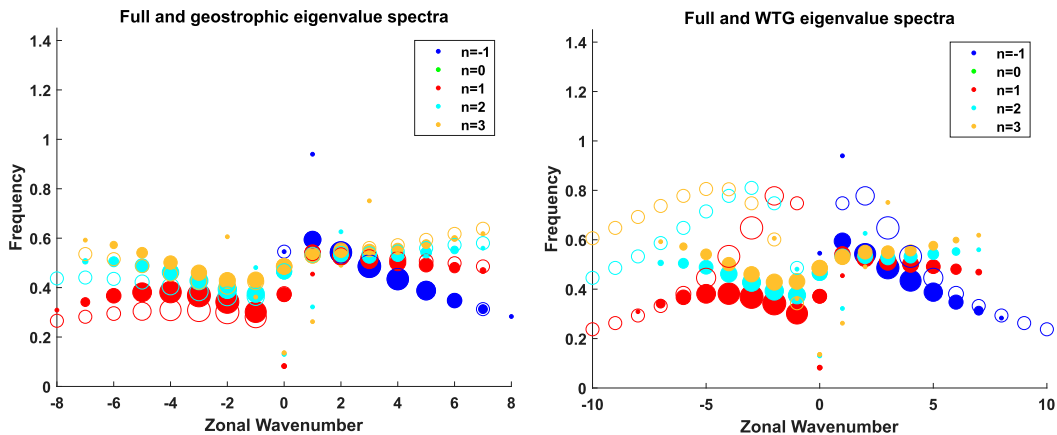


FIG. 6. As in Fig. 2, but also showing (left) the geostrophic approximation to the full solutions and (right) the solutions obtained using geostrophic and WTG approximations. The approximate solutions are shown by the open circles.

Acknowledgments. The author gratefully acknowledges the support of the National Science Foundation through Grant NSF AGS-1906768, as well as helpful comments by three anonymous reviewers.

Data availability statement: All of the data used in this paper are related to the eigenvalues and eigenfunctions of the linear model, which the user can reproduce using MATLAB codes available at <ftp://texmex.mit.edu/pub/emanuel/scripts/equapak.zip>.

REFERENCES

- Arnold, N. P., and D. A. Randall, 2015: Global-scale convective aggregation: Implications for the Madden-Julian oscillation. *J. Adv. Model. Earth Syst.*, **7**, 1499–1518, <https://doi.org/10.1002/2015MS000498>.
- Bony, S., and K. Emanuel, 2005: On the role of moist processes in tropical intraseasonal variability: Cloud–radiation and moisture–convection feedbacks. *J. Atmos. Sci.*, **62**, 2770–2789, <https://doi.org/10.1175/JAS3506.1>.
- Chumakova, L. G., R. R. Rosales, and E. G. Tabak, 2013: Leaky rigid lid: New dissipative modes in the troposphere. *J. Atmos. Sci.*, **70**, 3119–3127, <https://doi.org/10.1175/JAS-D-12-065.1>.
- Emanuel, K. A., 1987: An air–sea interaction model of intraseasonal oscillations in the tropics. *J. Atmos. Sci.*, **44**, 2324–2340, [https://doi.org/10.1175/1520-0469\(1987\)044<2324:AASIMO>2.0.CO;2](https://doi.org/10.1175/1520-0469(1987)044<2324:AASIMO>2.0.CO;2).
- , 1993: The effect of convective response time on WISHE modes. *J. Atmos. Sci.*, **50**, 1763–1776, [https://doi.org/10.1175/1520-0469\(1993\)050<1763:TEOCRT>2.0.CO;2](https://doi.org/10.1175/1520-0469(1993)050<1763:TEOCRT>2.0.CO;2).
- Fuchs, Z., and D. J. Raymond, 2005: Large-scale modes in a rotating atmosphere with radiative–convective instability and WISHE. *J. Atmos. Sci.*, **62**, 4084–4094, <https://doi.org/10.1175/JAS3582.1>.
- , and —, 2017: A simple model of intraseasonal oscillations. *J. Adv. Model. Earth Syst.*, **9**, 1195–1211, <https://doi.org/10.1002/2017MS000963>.
- Hendon, H. H., and B. Liebmann, 1994: Organization of convection within the Madden-Julian oscillation. *J. Geophys. Res.*, **99**, 8073–8083, <https://doi.org/10.1029/94JD00045>.
- Khairoutdinov, M. F., and K. Emanuel, 2018: Intraseasonal variability in a cloud-permitting near-global equatorial aquaplanet model. *J. Atmos. Sci.*, **75**, 4337–4355, <https://doi.org/10.1175/JAS-D-18-0152.1>.
- Kim, D., A. H. Sobel, and I.-S. Kang, 2011: A mechanism denial study on the Madden-Julian oscillation. *J. Adv. Model. Earth Syst.*, **3**, M12007, <https://doi.org/10.1029/2011MS000081>.
- Matsuno, T., 1966: Quasi-geostrophic motions in the equatorial area. *J. Meteor. Soc. Japan*, **44**, 25–43, https://doi.org/10.2151/jmsj1965.44.1_25.
- Neelin, J. D., and J. Yu, 1994: Modes of tropical variability under convective adjustment and the Madden-Julian oscillation. Part I: Analytical theory. *J. Atmos. Sci.*, **51**, 1876–1894, [https://doi.org/10.1175/1520-0469\(1994\)051<1876:MOTVUC>2.0.CO;2](https://doi.org/10.1175/1520-0469(1994)051<1876:MOTVUC>2.0.CO;2).
- Shi, X., D. Kim, Á. F. Adames, and J. Sukhatme, 2018: WISHE-moisture mode in an aquaplanet simulation. *J. Adv. Model. Earth Syst.*, **10**, 2393–2407, <https://doi.org/10.1029/2018MS001441>.
- Wheeler, M., and G. N. Kiladis, 1999: Convectively coupled equatorial waves: Analysis of clouds and temperature in the wavenumber–frequency domain. *J. Atmos. Sci.*, **56**, 374–399, [https://doi.org/10.1175/1520-0469\(1999\)056<0374:CCEWAO>2.0.CO;2](https://doi.org/10.1175/1520-0469(1999)056<0374:CCEWAO>2.0.CO;2).
- Yano, J.-I., and K. A. Emanuel, 1991: An improved WISHE model of the equatorial atmosphere and its coupling with the stratosphere. *J. Atmos. Sci.*, **48**, 377–389, [https://doi.org/10.1175/1520-0469\(1991\)048<0377:AIMOTE>2.0.CO;2](https://doi.org/10.1175/1520-0469(1991)048<0377:AIMOTE>2.0.CO;2).
- Zurovac-Jevtić, D., S. Bony, and K. Emanuel, 2006: On the role of clouds and moisture in tropical waves: A two-dimensional model study. *J. Atmos. Sci.*, **63**, 2140–2155, <https://doi.org/10.1175/JAS3738.1>.